Convergence Behavior and Acceleration of the Berenger and Leaky Modes Series Composing the 2-D Green's Function for the Microstrip Substrate

Hendrik Rogier, *Member, IEEE*, and Daniël De Zutter, *Fellow, IEEE*

***Abstract*—The Green's functions G_A and G_V are calculated for a two-dimensional microstrip substrate by placing the substrate into a closed perfectly-matched-layer waveguide and by performing a modal expansion in Berenger and leaky modes. It is shown that each series composing G_A and G_V has a particular convergence behavior when considering small lateral distances between the excitation and the observation points. It is then demonstrated that, by applying the Shanks transform to accelerate each series separately, a more efficient calculation for the Green's functions can be obtained than by direct computation of the series. The theory is illustrated by means of a representative example.**

***Index Terms*—Green's functions for multilayered media, integral equation techniques, perfectly matched layers.**

I. Introduction

ALTHOUGH the issue has been studied for quite a number of years, the calculation of the Green's functions G_A and G_V of a multilayered medium stills remains a difficult task. Yet, these kernel functions, associated with the vector and scalar potential of the problem, play a very important role in the so-called mixed-potential integral equation descriptions [1]–[3] of planar circuits, often used in computer-aided design (CAD) tools. It is well known [4], [5] that these Green's functions can be easily computed in the spectral domain; however, the inverse Fourier transform in two dimensions and the inverse Hankel transform in three dimensions lead to Sommerfeld-type of integrals, requiring complex and time-consuming integration schemes. Therefore, a number of faster alternative approaches has been proposed, such as, e.g., the fast Hankel transform [6] and the complex image technique [7], [8]. In [9]–[11], a new technique is proposed to calculate the Green's function by using perfectly matched layers (PMLs) [12]–[14], to obtain a closed waveguide configuration. The PML then mimics an open structure, while an efficient problem description in terms of a set of discrete modes of the closed waveguide containing the PML is possible.

Manuscript received September 21, 2001. The work of H. Rogier was supported by the Flemish Institute for the promotion of Scientific and Technological Research in the Industry (IWT) under a post-doctoral grant.

The authors are with the Information Technology Department, Ghent University, Ghent, Belgium (e-mail: hendrik.rogier@intec.rug.ac.be; daniel.dezutter@intec.rug.ac.be).

Publisher Item Identifier 10.1109/TMTT.2002.800389.

In [9]–[11], this approach is used to construct the Green's function G_{xx} for a two-dimensional (2-D) configuration for the TE polarization. In this paper, we will consider both TE and TM polarizations and derive modal series for the kernel functions G_A and G_V, often used in mixed-potential integral equation approaches for multilayered structures. An important issue concerning the use of modal series involves the number of modes needed to assure convergence of the series with a prescribed accuracy. The contributions of this paper relate to this convergence issue. First, a thorough convergence study is made on all modal series composing the Green's functions G_A and G_V. Second, the results of this study are then used to provide a series acceleration scheme by means of the Shanks transform.

In order not to complicate the matter too much, we will focus on a simple microstrip structure, and we chose a 2-D configuration. In order to develop our theory, we will make use of results obtained in [15], where it was shown that one can distinguish between leaky modes and Berenger modes in waveguides created by covering an open microstrip substrate with a PML. We start by briefly repeating this theory in Section II. The main part of the paper involves a thorough study on if, and how, the series converges when the lateral distance between the excitation and the observation points becomes small. In Section III, the kernel function G_A is treated , whereas in Section IV the Green's function G_V is considered. Finally, in Section V, the theory is illustrated on a representative microstrip substrate and the Shanks transform is proposed as an effective means to accelerate the modal series.

II. Modal Expansion for a Microstrip Substrate Terminated by a PML

Consider the configuration shown in Fig. 1, consisting of a microstrip substrate with permittivity ϵ_r, permeability μ_r, and thickness d. Above the substrate, an air region is present with thickness d_{air}, terminated by a PML with thickness d_{PML} and with material parameters κ_0 and σ_0 [9]. In [11], it is shown that, by stretching the coordinates, the air region can be combined with the PML to form a single air layer with complex thickness $\tilde{d} = d_{\text{air}} + d_{\text{PML}}(\kappa_0 - j(\sigma_0/\omega\epsilon_0))$. This allows a relatively simple modal analysis of the waveguide under consideration.

We are interested in the TE and TM modes of the configuration, propagating in the y direction with propagation constant

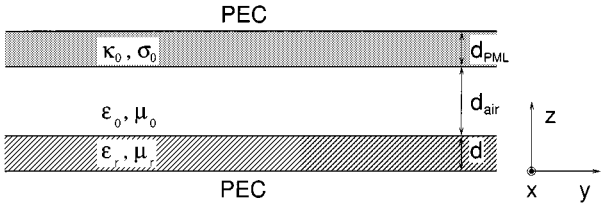

Fig. 1. Microstrip configuration.

β. For the TE eigenmode profiles, the relevant field component E_x is given by

$$E_x(y,\,z)=\begin{cases} A_{\rm TE}\sin(\gamma_r z)\sin\Big(\gamma_0\tilde{d}\Big)\,e^{-j\beta y}, \\ \qquad 0<z\le d \\ A_{\rm TE}\sin(\gamma_r d)\sin\Big[\gamma_0\Big(\tilde{d}+d-z\Big)\Big]\,e^{-j\beta y}, \\ \qquad d<z<d+d_{\rm air}. \end{cases} \tag{1}$$

For the TM eigenmode profiles, the relevant field component E_y is given by

$$E_y(y,\,z)=\begin{cases} -\dfrac{A_{\rm TM}\gamma_r}{j\omega\epsilon_0\epsilon_r}\sin(\gamma_r z)\cos\Big(\gamma_0\tilde{d}\Big)\,e^{-j\beta y}, \\ \qquad 0<z\le d \\ -\dfrac{A_{\rm TM}\gamma_r}{j\omega\epsilon_0\epsilon_r}\cot\Big(\gamma_0\tilde{d}\Big)\sin(\gamma_r d) \\ \quad\cdot\sin\Big[\gamma_0\Big(\tilde{d}+d-z\Big)\Big]\,e^{-j\beta y}, \\ \qquad d<z<d+d_{\rm air}. \end{cases} \tag{2}$$

For both polarizations, the constant A represents a normalization factor and γ_r and γ_0 satisfy a dispersion relation of the form

$$Y_r\cot(\gamma_r d)=-Y_0\cot\Big(\gamma_0\tilde{d}\Big) \tag{3}$$

with $\gamma_0^2=k_0^2-\beta^2$, $\gamma_r^2=k_0^2\epsilon_r\mu_r-\beta^2$, $k_0^2=\omega^2\epsilon_0\mu_0$, and with $Y_{r,\,\rm TE}=\gamma_r/j\omega\mu_0\mu_r$ and $Y_{0,\,\rm TE}=\gamma_0/j\omega\mu_0$ for the TE case, $Y_{r,\,\rm TM}=j\omega\epsilon_0\epsilon_r/\gamma_r$ and $Y_{0,\,\rm TM}=j\omega\epsilon_0/\gamma_0$ for the TM case. To assure propagation in the $+y$ direction with a bounded mode profile, the propagation constants must obey $\mathrm{Re}(\beta)\ge 0$ and $\mathrm{Im}(\beta)\le 0$. Branch cuts are then chosen so that $\mathrm{Re}(\gamma_r)$, $\mathrm{Re}(\gamma_0)\ge 0$ and $\mathrm{Im}(\gamma_r)$, $\mathrm{Im}(\gamma_0)\ge 0$.

In [15], it was shown that, when the PML acts as a strong absorber, the dispersion relation (3) allows us to distinguish between two sets of modes as follows.

1) The leaky modes of the microstrip substrate, for which most of the modal field is concentrated in the microstrip substrate, whilst the PML strongly attenuates the field. This corresponds to the assumption that $|\mathrm{Re}(\gamma_0)|d_{\rm PML}\sigma_0/\omega\epsilon_0$ is large and that

$$|\mathrm{Im}(\gamma_0)|\ll\frac{d_{\rm PML}\frac{\sigma_0}{\omega\epsilon_0}}{d_{\rm air}+d_{\rm PML}\kappa_0}\,|\mathrm{Re}(\gamma_0)|.$$

Under these assumptions and for $\mathrm{Re}(\gamma_0)>0$, (3) can be rewritten as

$$e^{-2j\gamma_r d}=\frac{Y_r+Y_0}{Y_0-Y_r}. \tag{4}$$

2) The Berenger modes, for which most of the modal field is concentrated in the PML, whilst a strong attenuation is found in the microstrip substrate. This is the case when $|\mathrm{Im}(\gamma_r)|d$ is large, so that (3) can be written as

$$e^{-2j\gamma_0\tilde{d}}=\frac{Y_r-Y_0}{Y_r+Y_0}. \tag{5}$$

Furthermore, analytic solutions were derived in [15] for the propagation constants of the leaky and Berenger modes in the quasi-static limit. The assumption that $\omega\sqrt{\epsilon_0\mu_0}\ll\beta$ then allows the approximation $\gamma_r\approx\gamma_0\approx+j\beta$. In the TE case, the propagation constants for the leaky modes are approximated by

$$\gamma_r\approx\begin{cases}\dfrac{1}{2jd}\log\left|\dfrac{\mu_r-1}{\mu_r+1}\right|+\dfrac{n\pi}{d}, & \mu_r\ne 1 \\ \dfrac{(2n+1)\pi}{2d}+j\,\dfrac{1}{d}\log\dfrac{(2n+1)\pi}{k_0 d\sqrt{\epsilon_r-1}}, & \mu_r=1.\end{cases} \tag{6}$$

For the Berenger modes, one finds

$$\gamma_0\approx\begin{cases}-\dfrac{1}{2j\tilde{d}}\log\left|\dfrac{\mu_r-1}{\mu_r+1}\right|+\dfrac{(2n+1)\pi}{2\tilde{d}}, & \mu_r\ne 1 \\ \dfrac{n\pi}{\tilde{d}}-j\,\dfrac{1}{\tilde{d}}\log\dfrac{2n\pi}{k_0\tilde{d}\sqrt{\epsilon_r-1}}, & \mu_r=1.\end{cases} \tag{7}$$

For the TM- polarization, the modal constants of the leaky modes are approximately equal to

$$\gamma_r\approx\frac{1}{2jd}\log\left|\frac{\epsilon_r-1}{\epsilon_r+1}\right|+\frac{(2n+1)\pi}{2d} \tag{8}$$

whereas for the Berenger modes

$$\gamma_0\approx-\frac{1}{2j\tilde{d}}\log\left|\frac{\epsilon_r-1}{\epsilon_r+1}\right|+\frac{n\pi}{\tilde{d}}. \tag{9}$$

III. Convergence Behavior of the Modal Series for G_A

By invoking the reciprocity theorem, the Green's function $G_A(y,\,z;\,y',\,z')$ for a line source at $(y',\,z')$ carrying an x-oriented current can now be expressed as a series of TE modes. For a source lying in or on top of the microstrip substrate ($0<z'\le d$), the Green's function in or on top of the substrate ($0<z\le d$) can be written as

$$\begin{aligned} &G_A(y,\,z;\,y',\,z') \\ &\quad=-\sum_{n=1}^{\infty}\frac{\omega\mu_0}{\beta} \\ &\qquad\cdot\frac{\sin(\gamma_r z)\sin(\gamma_r z')e^{-j\beta|y-y'|}}{\frac{d}{\mu_r}+\tilde{d}\,\frac{Y_0^2+Y_r^2}{2Y_0^2}-\frac{\gamma_0^2-\gamma_r^2}{\gamma_0 Y_0\mu_r}\frac{\sin(2\gamma_r d)}{2\gamma_r}-\frac{Y_0^2-Y_r^2}{Y_0^2}\frac{\tilde{d}}{2}\cos(2\gamma_r d)}, \\ &\qquad 0<z,\,z'\le d. \end{aligned} \tag{10}$$

Similar expressions can be found for excitation and/or observation points lying in the air region.

The series (10) clearly converges exponentially whenever excitation and observation points are well separated in the y direc-

tion, so that $|y-y'|$ is sufficiently large. At large distances, the main contributors to the modal series are the surface waves of the microwave structure, since these are guided without attenuation ($\mathrm{Im}(\beta)=0$). However, for sufficiently small distances $|y-y'|$, exponential convergence is lost, and the series becomes slowly converging or even divergent, making it a less efficient way to calculate the Green's function.

It is, therefore, instructive to study the convergence behavior of G_A for small $|y-y'|$. We start by subdividing the modal series (10) into a contribution $G_A^{(1)}$ of the leaky modes and a contribution $G_A^{(2)}$ of the Berenger modes. Whether a mode contributes to a leaky mode series or to the Berenger mode series depends on whether its modal constant is best approximated by the analytical expressions (6) or (7). For each contribution, an asymptotic series can be constructed for large n. When applying the assumptions for the leaky modes that led to (4), one obtains for the leaky mode part for the Green's function

$$G_A^{(1)}(y,\,z;\,y',\,z') \approx -\sum_{n=1}^{\infty} \frac{\omega\mu_0}{\beta}\, \frac{\sin(\gamma_r z)\sin(\gamma_r z')e^{-j\beta|y-y'|}}{\frac{d}{\mu_r}-\frac{\sin 2\gamma_r d}{2\gamma_r\mu_r}+\frac{\sin^2(\gamma_r d)}{j\gamma_0}}, \qquad 0<z,\,z'\le d. \tag{11}$$

For the contribution of the leaky modes to the Green's function at the substrate–air interface, which is in fact the worst case with respect to convergence, this series behaves as

$$G_A^{(1)}(y,\,d;\,y',\,d) \sim \begin{cases} \displaystyle\sum_{n=1}^{\infty} \frac{\omega\mu_0\mu_r}{(\mu_r^2-1)\beta\left(d+\frac{\mu_r(\epsilon_r\mu_r-1)}{j(\mu_r^2-1)\beta^2\gamma_0}\right)}\, e^{-j\beta|y-y'|}, \\ \qquad \mu_r\neq 1 \\ \displaystyle\sum_{n=1}^{\infty} -\frac{j\omega\mu_0\gamma_r}{k_0^2(\epsilon_r-1)\left(d+\frac{1}{j\gamma_0}\right)}\, e^{-j\beta|y-y'|}, \\ \qquad \mu_r=1. \end{cases} \tag{12}$$

These asymptotic expressions show that, for $\mu_r\neq 1$, the leaky mode series behaves as the harmonic series $\sum_n(1/n)$ in the absence of exponential damping when $y=y'$. This series is well known to be divergent. This is not unexpected, as a $\log|y-y'|$ singularity must be obtained for small values of $|y-y'|$. For $\mu_r=1$, the series behaves as $\sum_n n$, also clearly divergent in the absence of exponential damping. When $\mu_r=1$, an asymptotic expression can also be derived for the excitation and observation point not lying on the substrate–air interface, yielding

$$G_A^{(1)}(y,\,z;\,y',\,z') \sim \sum_{n=1}^{\infty} -e^{-j((2n+1)\pi(z+z'-2d)/2d)} \left(\frac{2\gamma_r}{k_0\sqrt{\epsilon_r-1}}\right)^{(z+z'-2d)/d} \cdot \frac{j\omega\mu_0\gamma_r}{k_0^2(\epsilon_r-1)\left(d+\frac{1}{j\gamma_0}\right)}\, e^{-j\beta|y-y'|}, \quad 0<z,\,z'\le d. \tag{13}$$

The series shows an additional oscillating factor and a damping factor whenever excitation or observation point are not placed on the substrate–air interface. Although the damping factor increases the convergence for small values of $|y-y'|$, the series still allows the presence of a singularity whenever $y=y'$ and $z=z'$. This singularity disappears for $z\neq z'$ due to the oscillating factor. As for the contribution of the Berenger modes to the Green's function, the assumptions leading to (5) yield

$$G_A^{(2)}(y,\,z;\,y',\,z') \approx -\sum_{n=1}^{\infty} \frac{\omega\mu_0}{\beta}\, \frac{\sin(\gamma_r z)\sin(\gamma_r z')}{\sin^2(\gamma_r d)} \cdot \frac{\sin^2\left(\gamma_0\tilde{d}\right)e^{-j\beta|y-y'|}}{\tilde{d}-\frac{\sin 2\gamma_0\tilde{d}}{2\gamma_0}-\frac{\sin^2\left(\gamma_0\tilde{d}\right)}{j\gamma_0}}, \qquad 0<z,\,z'\le d. \tag{14}$$

The following asymptotic behavior is observed for $z=z'=d$:

$$G_A^{(2)}(y,\,d;\,y',\,d) \approx \begin{cases} \displaystyle\sum_{n=1}^{\infty} -\frac{\omega\mu_0\mu_r^2}{(\mu_r^2-1)\beta\left(\tilde{d}-\frac{\mu_r(\epsilon_r\mu_r-1)}{j(\mu_r^2-1)\beta^2\gamma_0}\right)}\, e^{-j\beta|y-y'|}, \\ \qquad \mu_r\neq 1 \\ \displaystyle\sum_{n=1}^{\infty} \frac{j\omega\mu_0\gamma_0}{k_0^2(\epsilon_r-1)\left(\tilde{d}-\frac{1}{j\gamma_r}\right)}\, e^{-j\beta|y-y'|}, \\ \qquad \mu_r=1. \end{cases} \tag{15}$$

An asymptotic expression can also be given for the excitation and observation point not lying on the substrate–air interface, yielding in the region $0<z,\,z'\le d$

$$G_A^{(2)}(y,\,z;\,y',\,z') \sim \begin{cases} \displaystyle\sum_{n=1}^{\infty} -e^{j\gamma_0(z+z'-2d)} \frac{\omega\mu_0\mu_r^2}{(\mu_r^2-1)\beta\left(\tilde{d}-\frac{\mu_r(\epsilon_r\mu_r-1)}{j(\mu_r^2-1)\beta^2\gamma_0}\right)} \\ \qquad \cdot e^{-j\beta|y-y'|}, \qquad \mu_r\neq 1 \\ \displaystyle\sum_{n=1}^{\infty} e^{j\gamma_0(z+z'-2d)}\, \frac{j\omega\mu_0\gamma_0}{k_0^2(\epsilon_r-1)\left(\tilde{d}-\frac{1}{j\gamma_r}\right)}\, e^{-j\beta|y-y'|}, \\ \qquad \mu_r=1. \end{cases} \tag{16}$$

This clearly shows that the Berenger mode part of the series has an additional exponential damping, guaranteeing convergence whenever the excitation and/or observation point is lying in the region $0<z,\,z'<d$, and not on the interface.

IV. Convergence Behavior of the Modal Series for G_V

In a similar fashion as for G_A, the reciprocity theorem can be invoked to construct the Green's function $G_V(y,\,z;\,y',\,z')$ for a line charge as a series of TE and TM modes. For a source lying in the microstrip substrate, i.e., for $0<z,\,z'\le d$, the Green's function in the substrate can be written as (17), shown at the bottom of the following page. Similar expressions can be found for excitation and/or observation points lying in the air region.

Concerning the convergence behavior of the modal series, the same observations hold as in the previous section. Better insight can be gained by studying the TE and TM series separately and by subdividing both of them in a series belonging to the leaky modes and a series describing the contribution of the Berenger

modes. Concerning the convergence of the TE part, similar expressions can be derived as the ones found in the previous section, provided the extra β_{TE}^2 term in the denominator is taken into account. For $\mu_r = 1$, for example, the following asymptotic expression can be derived for the leaky mode part in the region $0 < z, z' \leq d$:

$$G_{V,\mathrm{TE}}^{(1)}(y, z; y', z') \sim \sum_{n=1}^{\infty} e^{-j((2n+1)\pi(z+z'-2d)/2d)} \left(\frac{2\gamma_r}{k_0\sqrt{(\epsilon_r-1)}} \right)^{(z+z'-2d)/d} \cdot \frac{j\omega\mu_0}{\gamma_r k_0^2(\epsilon_r-1)\left(d+\frac{1}{j\gamma_0}\right)} e^{-j\beta|y-y'|}. \tag{18}$$

On the other hand, the Berenger part behaves as

$$G_{V,\mathrm{TE}}^{(2)}(y, z; y', z') \sim \begin{cases} \displaystyle\sum_{n=1}^{\infty} - e^{j\gamma_0(z+z'-2d)} \frac{\omega\mu_0\mu_r^2}{(\mu_r^2-1)\beta^3\left(\tilde{d} - \frac{\mu_r(\epsilon_r\mu_r-1)}{j(\mu_r^2-1)\beta^2\gamma_0}\right)} \cdot e^{-j\beta|y-y'|}, & \mu_r \neq 1 \\ \displaystyle\sum_{n=1}^{\infty} - e^{j\gamma_0(z+z'-2d)} \frac{j\omega\mu_0}{k_0^2(\epsilon_r-1)\gamma_r\left(\tilde{d} - \frac{1}{j\gamma_r}\right)} \cdot e^{-j\beta|y-y'|}, & \mu_r = 1. \end{cases} \tag{19}$$

Let us now further concentrate on the TM contribution. When applying the assumptions for the leaky modes that led to (4), one obtains for the leaky mode part

$$G_{V,\mathrm{TM}}^{(1)}(y, z; y', z') \approx \sum_{n=1}^{\infty} \frac{\gamma_r^2}{\beta^3\omega\epsilon_0\epsilon_r^2} \frac{\sin(\gamma_r z)\sin(\gamma_r z')e^{-j\beta|y-y'|}}{\frac{d}{\epsilon_r} + \frac{\sin 2\gamma_r d}{2\gamma_r\epsilon_r} + \frac{\cos^2(\gamma_r d)}{j\gamma_0}}, \quad 0 < z, z' \leq d. \tag{20}$$

At the substrate–air interface, the series of leaky modes behaves as

$$G_{V,\mathrm{TM}}^{(1)}(y, d; y', d) \sim \sum_{n=1}^{\infty} -\frac{1}{\beta\omega\epsilon_0(\epsilon_r^2-1)} \frac{e^{-j\beta|y-y'|}}{\frac{d}{\epsilon_r} - \frac{k_0^2(\epsilon_r\mu_r-1)}{j\gamma_0\gamma_r^2(\epsilon_r^2-1)}}. \tag{21}$$

Concerning the Berenger mode part, the assumptions leading to (5) yield

$$G_{V,\mathrm{TM}}^{(2)}(y, z; y', z') \approx \sum_{n=1}^{\infty} \frac{\gamma_r^2}{\beta^3\omega\epsilon_0\epsilon_r^2} \frac{\sin(\gamma_r z)\sin(\gamma_r z')}{\sin^2(\gamma_r d)} \cdot \frac{\sin^2\left(\gamma_0\tilde{d}\right) e^{-j\beta|y-y'|}}{\tilde{d} + \frac{\sin 2\gamma_0\tilde{d}}{2\gamma_0} - \frac{\cos^2(\gamma_0\tilde{d})}{j\gamma_r\epsilon_r}}, \quad 0 < z, z' \leq d. \tag{22}$$

At the substrate–air interface and for large n, this series behaves as

$$G_{V,\mathrm{TM}}^{(2)}(y, d; y', d) \sim \sum_{n=1}^{\infty} \frac{1}{\beta\omega\epsilon_0(\epsilon_r^2-1)} \frac{e^{-j\beta|y-y'|}}{\tilde{d} + \frac{k_0^2\epsilon_r(\epsilon_r\mu_r-1)}{j\gamma_r\gamma_0^2(\epsilon_r^2-1)}}. \tag{23}$$

Similar to the TE series, the Berenger mode part of the series has additional exponential damping whenever excitation and/or observation point are lying in the region $0 < z, z' < d$, and not on the interface

$$G_{V,\mathrm{TM}}^{(2)}(y, z; y', z') \sim \sum_{n=1}^{\infty} e^{j\gamma_0(z+z'-2d)} \frac{1}{\beta\omega\epsilon_0(\epsilon_r^2-1)} \frac{e^{-j\beta|y-y'|}}{\tilde{d} + \frac{k_0^2\epsilon_r(\epsilon_r\mu_r-1)}{j\gamma_r\gamma_0^2(\epsilon_r^2-1)}}, \quad 0 < z, z' \leq d. \tag{24}$$

V. Example

In order to illustrate the theory developed in the previous sections, we consider a microstrip-PML configuration with $d = 9$ mm, $d_{\mathrm{air}} = 5$ mm, and $d_{\mathrm{PML}} = 3.5$ mm at 12 GHz. A strongly absorbing PML is obtained for $\kappa_0 = 10$ and $\sigma_0/\omega\epsilon_0 = 8$. The modal series are then constructed for the Green's functions G_A and G_V of a microstrip substrate with $\epsilon_r = 3$ and $\mu_r = 1$. In [15], the exact locations of the propagation constants of the TE and TM modes were given for this substrate, as well as the eigenvalues found with the approximate analytical expressions, allowing us to distinguish between zeros pertaining to leaky and Berenger modes.

A. Behavior of the Modal Series' Coefficients

In Figs. 2–9, the convergence behavior of the coefficients is shown for the different modal series that compose G_A and G_V, assuming that $|y - y'| = 0$. In Figs. 2 and 3, it is shown that the real and imaginary parts of the coefficients for the leaky

$$G_V(y, z; y', z') = -\sum_{n=1}^{\infty} \frac{\omega\mu_0}{\beta_{\mathrm{TE}}^3} \frac{\sin(\gamma_{r,\mathrm{TE}} z)\sin(\gamma_{r,\mathrm{TE}} z')e^{-j\beta_{\mathrm{TE}}|y-y'|}}{\frac{d}{\mu_r} + \tilde{d}\frac{Y_{0,\mathrm{TE}}^2+Y_{r,\mathrm{TE}}^2}{2Y_{0,\mathrm{TE}}^2} - \frac{\gamma_{0,\mathrm{TE}}^2-\gamma_{r,\mathrm{TE}}^2}{\gamma_{0,\mathrm{TE}}Y_{0,\mathrm{TE}}\mu_r}\frac{\sin(2\gamma_{r,\mathrm{TE}}d)}{2\gamma_{r,\mathrm{TE}}} - \frac{Y_{0,\mathrm{TE}}^2-Y_{r,\mathrm{TE}}^2}{Y_{0,\mathrm{TE}}^2}\frac{\tilde{d}}{2}\cos(2\gamma_{r,\mathrm{TE}}d)} + \sum_{n=1}^{\infty} \frac{\gamma_{r,\mathrm{TM}}^2}{\beta_{\mathrm{TM}}^3\omega\epsilon_0\epsilon_r^2} \frac{\sin(\gamma_{r,\mathrm{TM}} z)\sin(\gamma_{r,\mathrm{TM}} z')e^{-j\beta_{\mathrm{TM}}|y-y'|}}{\frac{d}{\epsilon_r} + \tilde{d}\frac{Y_{0,\mathrm{TM}}^2+Y_{r,\mathrm{TM}}^2}{2Y_{r,\mathrm{TM}}^2} - \frac{Y_{0,\mathrm{TM}}\gamma_{r,\mathrm{TM}}\epsilon_r - Y_{r,\mathrm{TM}}\gamma_{0,\mathrm{TM}}}{2Y_{r,\mathrm{TM}}\gamma_{0,\mathrm{TM}}}\frac{\sin(2\gamma_{r,\mathrm{TM}}d)}{2\gamma_{r,\mathrm{TM}}\epsilon_r} - \frac{Y_{0,\mathrm{TM}}^2-Y_{r,\mathrm{TM}}^2}{Y_{r,\mathrm{TM}}^2}\frac{\tilde{d}}{2}\cos(2\gamma_{r,\mathrm{TM}}d)} \tag{17}$$

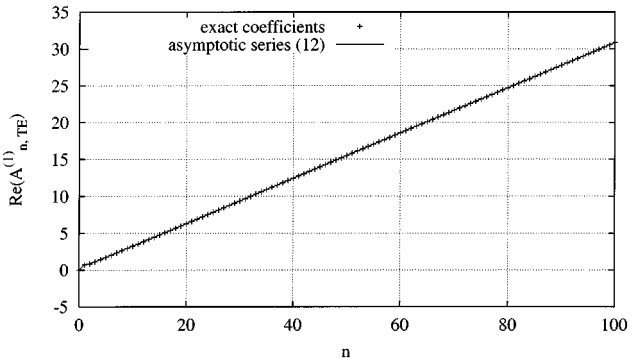

Fig. 2. Convergence behavior of the real part of the coefficients in the leaky mode series for $G_A(y,\ d;\ y,\ d)$.

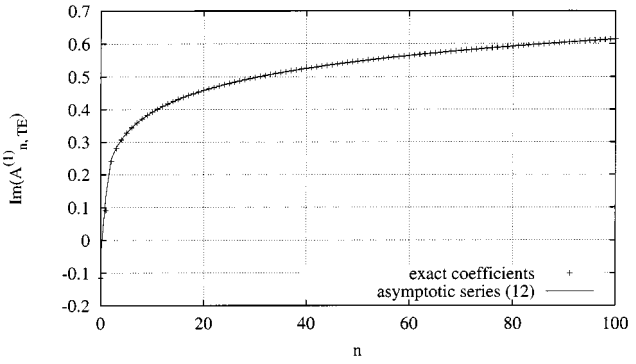

Fig. 3. Convergence behavior of the imaginary part of the coefficients in the leaky mode series for $G_A(y,\ d;\ y,\ d)$.

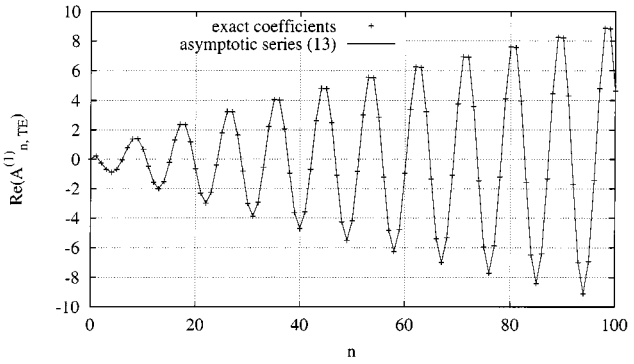

Fig. 4. Convergence behavior of the real part of the coefficients in the leaky mode series for $G_A(y,\ z_0;\ y,\ d)$.

mode series $G_A^{(1)}(y,\ d;\ y,\ d) = \sum_{n-1}^{\infty} A_{n,\mathrm{TE}}^{(1)}$ contributing to $G_A(y,\ d;\ y,\ d)$ approach the asymptotic series (12) for sufficiently large n (difference $< 1\%$ for $n \geq 8$). The same holds when the observation point is chosen inside the substrate for $z = z_0 = 7$ mm, and the asymptotic expression (13) is used. In Figs. 4 and 5, the oscillatory character is clearly visible and the series increases less than linear with n.

In Figs. 6 and 7, the asymptotic behavior is illustrated for the real and imaginary parts of the coefficients for the Berenger mode series $G_A^{(2)}(y,\ d;\ y,\ d) = \sum_{n-1}^{\infty} A_{n,\mathrm{TE}}^{(2)}$ contributing to $G_A(y,\ d;\ y,\ d)$, exhibiting a linear behavior for large n, following (15).

Concerning the series contributing to $G_V(y,\ z,\ y',\ z')$, similar observations can be made. Let us not expand on this any

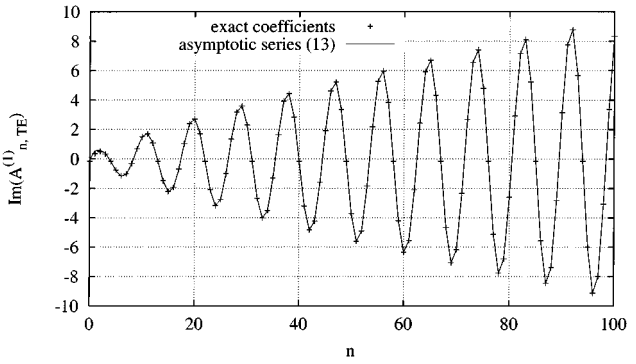

Fig. 5. Convergence behavior of the imaginary part of the coefficients in the leaky mode series for $G_A(y,\ z_0;\ y,\ d)$.

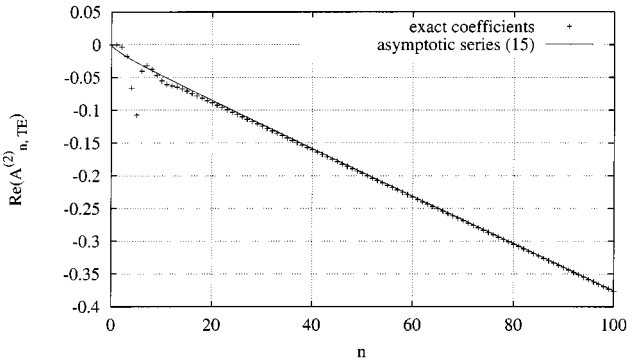

Fig. 6. Convergence behavior of the real part of the coefficients in the Berenger mode series for $G_A(y,\ d;\ y,\ d)$.

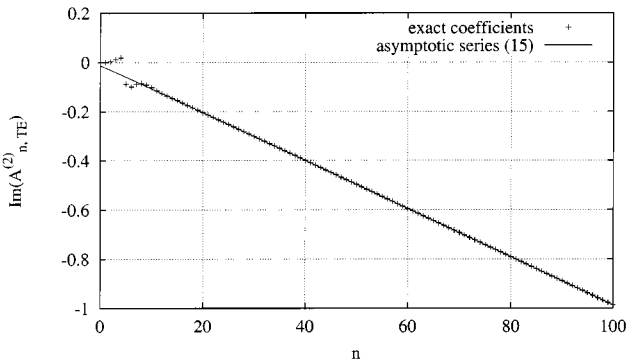

Fig. 7. Convergence behavior of the imaginary part of the coefficients in the Berenger mode series for $G_A(y,\ d;\ y,\ d)$.

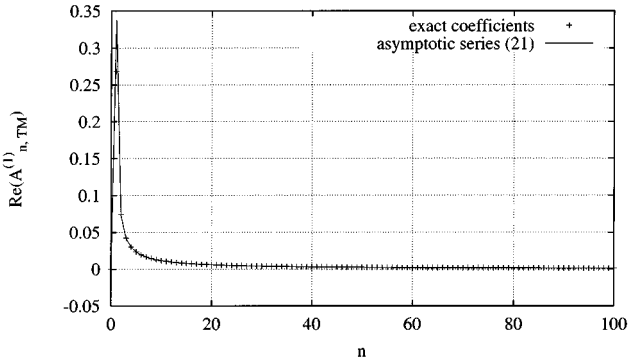

Fig. 8. Convergence behavior of the real part of the coefficients in the leaky TM mode series for $G_V(y,\ d;\ y,\ d)$.

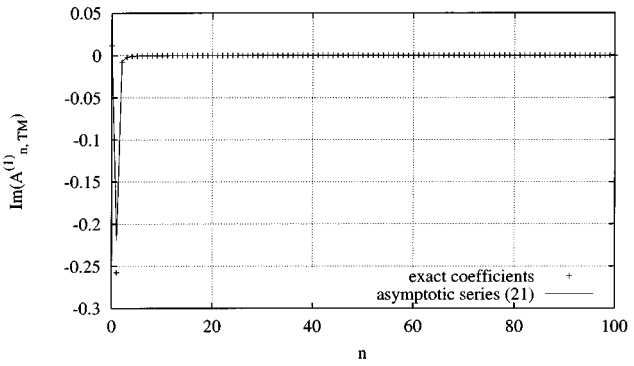

Fig. 9. Convergence behavior of the imaginary part of the coefficients in the leaky TM mode series for $G_V(y,\, d;\, y,\, d)$.

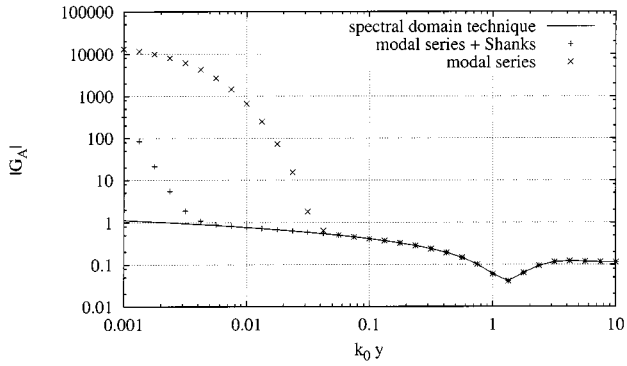

Fig. 10. Green's function $G_A(y,\, d;\, 0,\, d)$ at the microstrip–air interface.

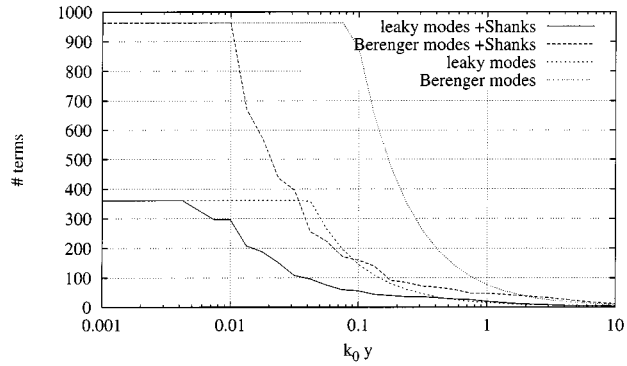

Fig. 11. Number of terms needed in the modal series contributing to $G_A(y,\, d;\, 0,\, d)$.

further and simply show, e.g., the asymptotic behavior for the leaky TM mode series $G^{(1)}_{V,\mathrm{TM}}(y,\, d;\, y,\, d) = \sum_{n-1}^{\infty} A^{(1)}_{n,\mathrm{TM}}$ in Figs. 8 and 9, corresponding to the $1/n$ behavior of (21) for large n.

B. Calculation of the Green's Functions and Series Acceleration by Shanks Transformation

Sections III and IV clearly showed that the modal expansions for the Green's functions G_A and G_V are rapidly converging whenever excitation and observation points are well separated in the y direction (large $|y-y'|$), but that convergence tends to slow down or to get lost when the distance $|y-y'|$ decreases. This is due to the following. For small n, the series of leaky modes consists of a number of modes that are either guided or only weakly evanescent. For increasing n, the modes in the leaky modes and Berenger modes series become more and more evanescent, so that only a small number of modes determines the field behavior for large $|y-y'|$. However, for decreasing $|y-y'|$ distances an increasing number of evanescent high-order is contributing significantly to the Green's function series. However, the efficiency of the modal series can be increased by well-known series acceleration techniques. We will show that the convergence speed can be drastically increased by applying the Shanks transform [16]. Since this algorithm is welldocumented in literature, we will not elaborate on its implementation details. Since each part that composes the Green's function G_A or G_V clearly has a distinct convergence behavior, the acceleration technique is applied to each separate series with TE or TM contributions from the Berenger or leaky modes.

Let us now investigate the calculation of the accelerated modal series for G_A and G_V, by applying (10) and (17). Special attention is paid to the behavior of the series for small values of $|y-y'|$, thereby examining the statements made in Sections III and IV and checking the effect of series acceleration by the Shanks transform. Before evaluating G_A and G_V, the propagation constants and normalization factors were computed for 359 leaky modes and 961 Berenger modes in the TE case and for 323 leaky modes and 948 Berenger modes in the TM case. Results are stored in a database and can be reused for all calculations of G_A and G_V for one particular substrate.

In Fig. 10, the amplitude of the Green's function $G_A(y,\, d;\, 0,\, d)$ on the microstrip–air interface is shown. A comparison is made between a classical calculation scheme, which relies on a spectral domain approach and inverse Fourier transform to the spatial domain [4], [5], and the modal series approach. Both direct calculation of the leaky mode and Berenger mode series composing G_A and the use of the Shanks transform to accelerate convergence of both series are considered. With the number of modes available in the database, direct computation of the two modal series gives acceptable results for $k_0 y \geq 0.1$, whereas with the use of series acceleration there is a good agreement with the spectral domain approach for values of $k_0 y$ up to 0.01. The effect of the Shanks transform can further be clarified by considering the number of terms used in the different series to obtain a relative accuracy of 10^{-7}, as shown in Fig. 11. It is clear that the number of terms needed for convergence is larger in a direct computation scheme than whenever Shanks acceleration is applied. This is especially the case for small values of $k_0 y$. For $k_0 y \leq 0.1$ both the number of leaky and Berenger modes available in the database are not sufficient to obtain the required accuracy. When making use of the Shanks transform, this phenomenon is only seen for $k_0 y \leq 0.01$.

Let us now consider the observation point inside the substrate at $z = z_0 = 7$ mm. $G_A(y,\, z_0;\, 0,\, d)$ is depicted in Fig. 12. In this case, the Green's function does not have a singular behavior for $y = y'$, and the modal series calculated with Shanks acceleration agrees well with the results of the spectral domain approach. However, diverging results are still obtained with direct calculation of the modal series. This is further illustrated in Fig. 13. As shown by (16), the additional exponential damping

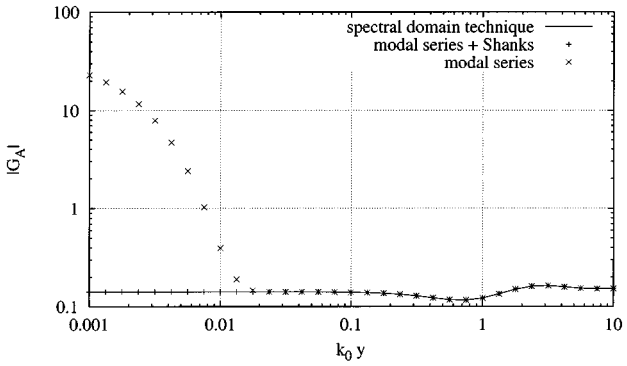

Fig. 12. Green's function $G_A(y, z_0; 0, d)$ for a source at the interface and the observation point inside the substrate.

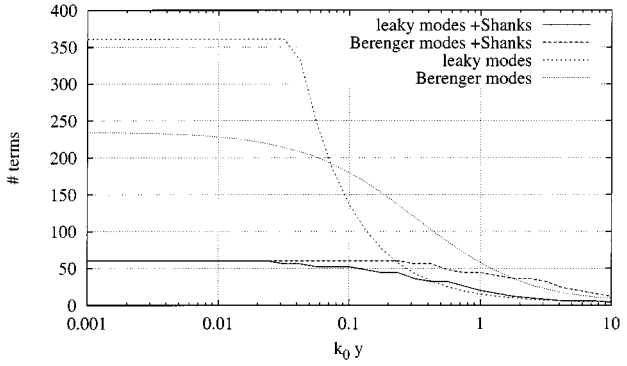

Fig. 13. Number of terms needed in the modal series contributing to $G_A(y, z_0; 0, d)$.

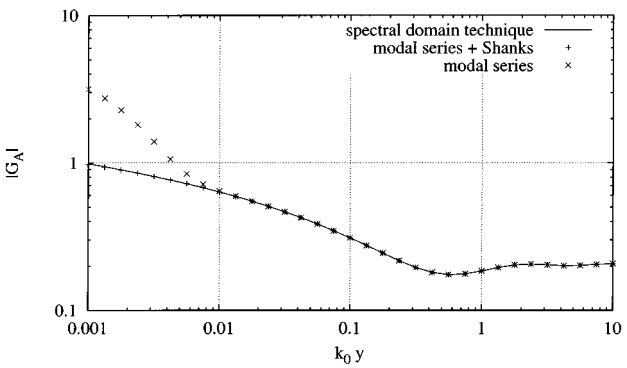

Fig. 14. Green's function $G_A(y, z_0, 0, z_0)$ for excitation and observation point inside the substrate.

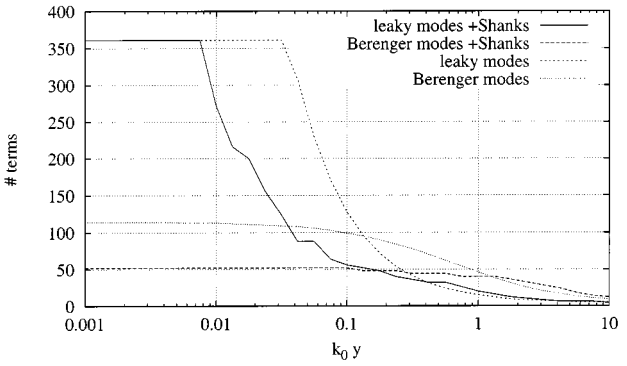

Fig. 15. Number of terms needed in the modal series contributing to $G_A(y, z_0; 0, z_0)$.

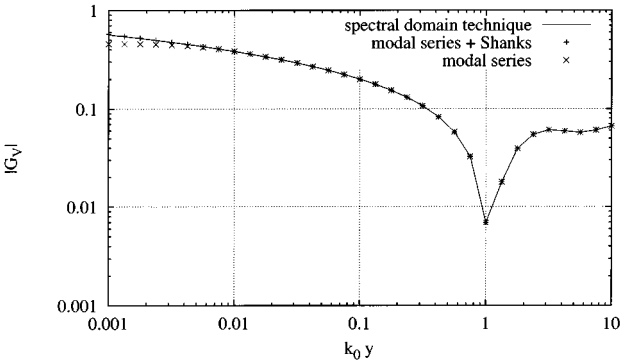

Fig. 16. Green's function $G_V(y, d; 0, d)$ at the microstrip–air interface.

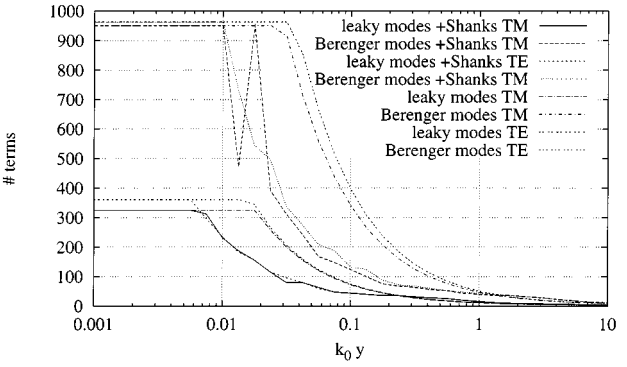

Fig. 17. Number of terms needed in the modal series contributing to $G_V(y, d; 0, d)$.

factor for $z \neq d$ leads to a series of Berenger modes that converges much faster for small values of $k_0 y$ than for $z = d$. However, the number of leaky modes available in the database remain insufficient to obtain an accuracy of 10^{-7} when direct computation is applied. Indeed, the additional damping obtained in (13) is not sufficient to allow fast convergence of this series. In any case, using Shanks transform drastically reduces the number of modes needed to obtain convergence.

Let us finally observe the modal series behavior for excitation and observation points both at $z = z' = z_0$, leading to a singular behavior of $G_A(y, z_0, 0, z_0)$ for $y = 0$. In Fig. 14, no noticeable difference is seen between the spectral domain approach and the modal technique with Shanks acceleration for $G_A(y, z_0; 0, z_0)$ calculated for $k_0 y > 0.001$. However, Fig. 15 shows that the leaky mode series does not provide a 10^{-7} accuracy for $k_0 y < 0.01$, even when applying Shanks acceleration. On the other hand, the series of Berenger series remains convergent, as elucidated by (16).

Similar effects can now be seen for the modal series composing G_V. Of course, because of the presence of the additional $1/\beta^2$ in combination with the fact that $\epsilon_r \neq 1$, the series composing G_V will in general behave better than the ones composing G_A, especially when $\mu_r = 1$. This is, for example, illustrated in Fig. 16, where $G_V(y, d; 0, d)$ at the microstrip–air interface is shown. Fig. 17 shows that the use of Shanks acceleration on the four different series composing $G_V(y, d; 0, d)$ assures an accuracy of 10^{-7} for $k_0 y > 0.01$, taking into account the number of TE and TM modes available in the database.

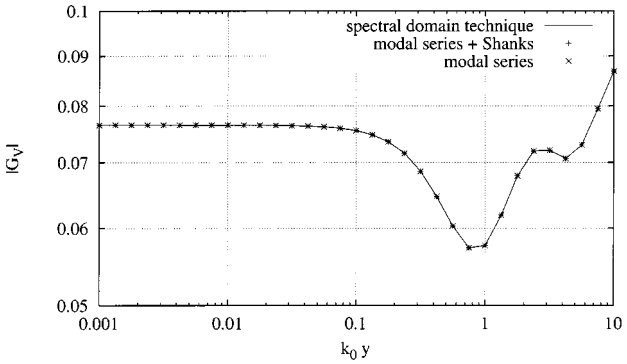

Fig. 18. Green's function $G_V(y,\ z_0;\ 0,\ d)$ for a source at the interface and the observation point inside the substrate.

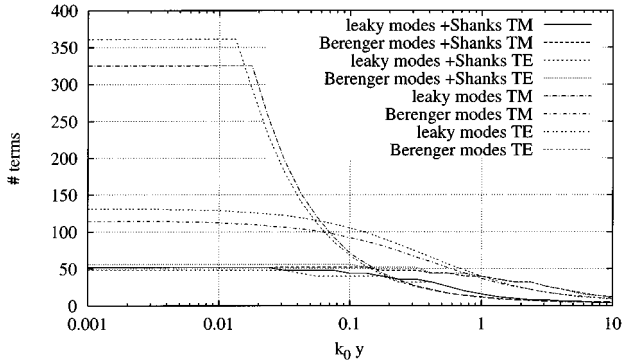

Fig. 19. Number of terms needed in the modal series contributing to $G_V(0,\ y_0;\ 0,\ d)$.

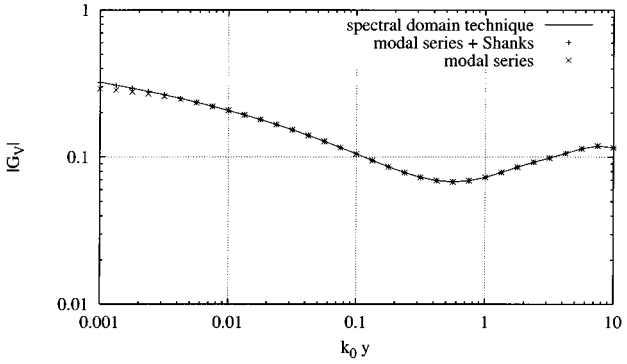

Fig. 20. Green's function $G_V(y,\ z_0;\ 0,\ z_0)$ for excitation and observation point inside the substrate.

For the observation point inside the substrate at $z = z_0 = 7$ mm, good agreement is seen for $G_V(y,\ z_0;\ 0,\ d)$ whenever $k_0 y \geq 0.001$, as shown in Fig. 18. However, Fig. 19 shows that direct computation does not allow us to obtain a 10^{-7} accuracy in the range $0.001 < k_0 y < 0.01$. In Fig. 20, $G_V(y,\ z_0;\ 0,\ z_0)$ is shown, for excitation and observation points both at $z = z' = z_0$, leading to a singular behavior for $y = 0$. On the one hand, both series of Berenger modes remain convergent, as seen in Fig. 21, because of the additional exponential damping as found in (16) and (24). Convergence is also seen for the leaky mode

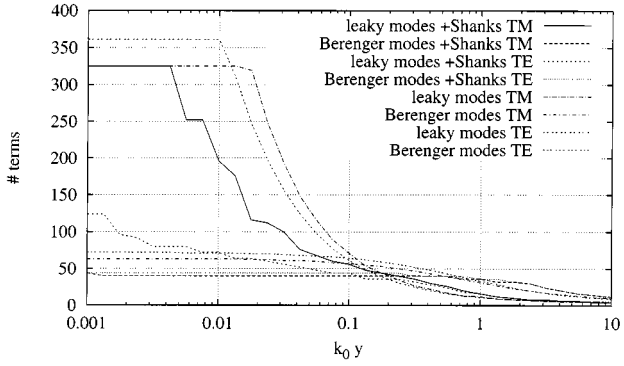

Fig. 21. Number of terms needed in the modal series contributing to $G_V(y,\ z_0;\ 0,\ z_0)$.

series in the TE case. This can be explained by considering (19). This expression shows that the series converges as

$$\sum_n \frac{1}{n^{(z+z'-3d)/d}}$$

which is a convergent series whenever z or z' are smaller than d. On the other hand, the leaky mode series in the TM case, however, does not acquire the prescribed accuracy for small values of $k_0 y$.

VI. Conclusion

The Green's functions G_A and G_V were calculated for a 2-D microstrip substrate by placing the substrate into a closed PML waveguide and by performing a modal expansion in Berenger and leaky modes. It is shown that each series composing G_A and G_V has a particular convergence behavior, depending on the position of the excitation and the observation points, the magnetic and dielectric contrasts in the substrate, and the type of modes under consideration. It is, therefore, necessary to accelerate the convergence of each separate series of modes by applying the Shanks transform. This clearly leads to a more efficient calculation of the Green's functions than by direct computation of the modal series, as shown by a representative example. The Shanks transform leads to accurate results when excitation and observation points approach each other, even for small distances of the order of $\lambda/100$. The technique, however, does not provide correct results for the self-patch contribution. There, a static approximation, exhibiting the correct singular behavior, could be used to evaluate the Green's functions efficiently.

Because of the exponential damping of the modes, only a very small number of mode terms is required when the excitation and the observation points are separated by more than $\lambda/5$, resulting in a very efficient method. Compared to the complex image method, our technique is theoretically founded and probably more efficient in 2-D since the complex image method yields an expansion in Hankel functions. For the moment, research is underway to extend the technique to three-dimensional (3-D). A drawback of the technique in 3-D is the fact that our modal series then requires Hankel functions, in contrast to the 3-D complex image method.

REFERENCES

[1] N. Faché, F. Olyslager, and D. De Zutter, *Electromagnetic and Circuit Modeling of Multiconductor Transmission Lines*. New York: Oxford Sci., 1993.

[2] J. Sercu, N. Faché, F. Libbrecht, and P. Lagasse, "Mixed potential integral equation technique for hybrid microstrip-slotline multilayered circuits using a mixed rectangular-triangular mesh," *IEEE Trans. Microwave Theory Tech.*, vol. 43, pp. 1162–1172, May 1995.

[3] J. R. Mosig, *Numerical Techniques for Microwave and Millimeter-Wave Passive Structures*, T. Itoh, Ed. New York: Wiley, 1988, ch. Integral Equation Techniques.

[4] K. A. Michalski and J. R. Mosig, "Multilayer media Green's functions in integral equation formulations," *IEEE Trans. Antennas Propagat.*, vol. 45, pp. 508–519, Mar. 1997.

[5] N. Faché, J. Van Hese, and D. De Zutter, "Generalized space domain Green's dyadic for multilayered media with special application to microwave interconnections," *J. Electromagn. Waves Appl.*, vol. 3, no. 7, pp. 651–669, 1992.

[6] R. C. Hsieh and J. T. Kuo, "Fast full-wave analysis of planar microstrip circuit elements in stratified media," *IEEE Trans. Microwave Theory Tech.*, vol. 46, pp. 1291–1297, Sept. 1998.

[7] Y. L. Chow, J. J. Yang, D. G. Fang, and G. E. Howard, "A closed-form spatial Green's function for the thick microstrip substrate," *IEEE Trans. Microwave Theory Tech.*, vol. 39, pp. 588–592, Mar. 1991.

[8] J. Van Hese, H. Rogier, K. Blomme, and N. Faché, "Calculcation of spatial Green's functions: Numerical integration of Sommerfeld integrals versus complex image technique," in *Prog. Electrom. Res. Symp.*, July 1994, p. 299.

[9] H. Derudder, F. Olyslager, and D. De Zutter, "An efficient series expansion for the 2D Green's function of a microstrip substrate using perfectly matched layers," *IEEE Microwave Guided Wave Lett.*, vol. 9, pp. 505–507, Dec. 1999.

[10] P. Bienstman, H. Derudder, R. Baets, F. Olyslager, and D. De Zutter, "Analysis of cylindrical waveguide discontinuities using vectorial eigenmodes and perfectly matched layers," *IEEE Trans. Microwave Theory Tech.*, vol. 49, pp. 349–354, Feb. 2001.

[11] H. Derudder, F. Olyslager, D. De Zutter, and S. Van den Berghe, "Efficient mode-matching analysis of discontinuities in finite planar substrates using perfectly matched layers," *IEEE Trans. Antennas Propagat.*, vol. 49, pp. 1985–195, Feb. 2001.

[12] J. P. Bérenger, "Perfectly matched layer for the FDTD solution of wave-structure interaction problems," *IEEE Trans. Antennas Propagat.*, vol. 44, pp. 110–117, Jan. 1996.

[13] S. D. Gedney, "An anisotropic PML absorbing media for the FDTD simulation of fields in lossy and dispersive media," *Electromagnetics*, vol. 16, pp. 399–415, 1996.

[14] L. Knockaert and D. De Zutter, "On the stretching of Maxwell's equations in general orthogonal coordinate systems and the perfectly matched layer," *Microwave Opt. Technol. Lett.*, vol. 24, no. 1, pp. 31–34, Jan. 2000.

[15] H. Rogier and D. De Zutter, "Berenger and leaky modes in microstrip substrates terminated by a perfectly matched layer," *IEEE Trans. Microwave Theory Tech.*, vol. 49, pp. 712–715, Apr. 2001.

[16] S. Singh and R. Singh, "Application of transforms to accelarate the summation of periodic free-space Green's function," *IEEE Trans. Microwave Theory Tech.*, vol. 38, pp. 1746–1748, Nov. 1990.

Hendrik Rogier (S'96–A'99–M'00), photograph and biography not available at the time of publication.

Daniël De Zutter (M'92–SM'96–F'01), photograph and biography not available at the time of publication.